Neutrinos from the milky way

Visser, E.L.

6 DETECTION POTENTIAL OF KM3NET FOR THE DIFFUSE GALACTIC NEUTRINO FLUX

From the sensitivities and limits obtained with the ANTARES detector it can be concluded that a much bigger neutrino telescope is needed to probe the diffuse Galactic neutrino flux. The level of the flux that can be probed with ANTARES is more than a factor of 10 above the predicted fluxes.

The KM3NeT detector, which is the next generation neutrino telescope in the Mediterranean, is well suited to perform a measurement of the diffuse Galactic neutrino flux. Like ANTARES, its location in the Mediterranean Sea yields a high visibility of the region from which the highest signal is expected. Furthermore, the effective area is expected to be about two orders of magnitude bigger than that of ANTARES. A brief description of KM3NeT is given in section 6.1.

The analysis for KM3NeT is based on that developed for ANTARES. The number of events from the signal region is compared to the number of events from the background regions. These signal and background regions are constructed in the same way as done for ANTARES. The optimal size of the signal region for KM3NeT could be different than obtained for ANTARES. This potential difference is addressed in section 6.2. In section 6.3, the resulting sensitivity of KM3NeT is presented and compared to the limits and sensitivities obtained with ANTARES.

In addition to calculating the flux sensitivity of KM3NeT, the discovery potential is also assessed. This is described in more detail in section 6.4.

6.1 KM3NET

The KM3NeT detector will consist of neutrino telescopes at three sites in the Mediterranean Sea. The sites have been chosen after long-term site characterisation by the ANTARES, NEMO [Riccobene et al., 2005] and NESTOR [Belias et al., 2007] collaborations, and are selected according to several criteria. A suitable site should have a sufficient depth in order to provide shielding against atmospheric muons and at the same time be close to the coast, to ease deployment and reduce the costs of power and signal connections to shore. Furthermore, the optical properties of

NEMO: NEutrino Mediterranean Observatory

NESTOR: Neutrino Extended Submarine Telescope with Oceanographic Research

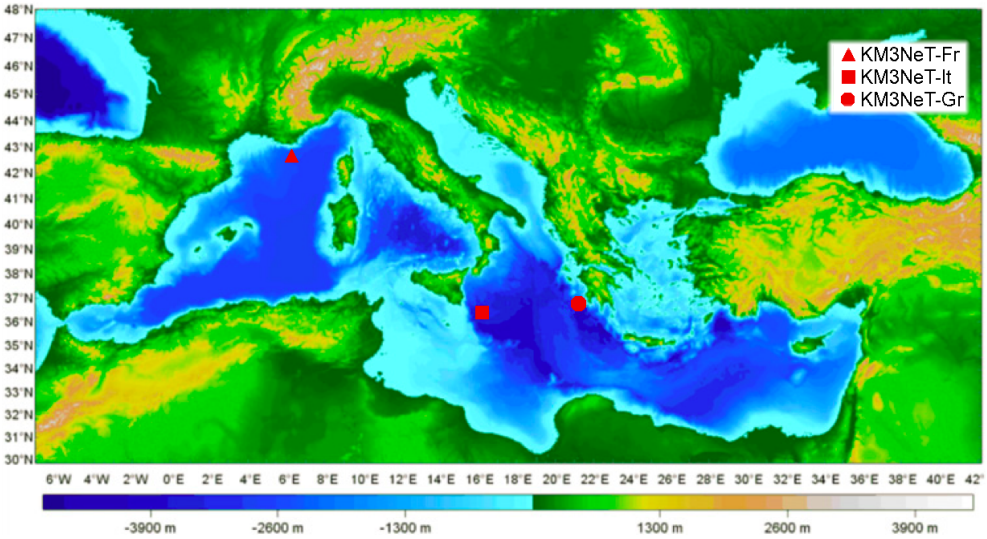

Figure 6.1: Bathymetry map of the Mediterranean Sea with the three site locations of KM3NeT marked. Figure reproduced from Margiotta [2013].

the water should be good (i. e. absorption and scattering lengths close to those of pure sea water) and the level of bioluminescence should be low.

The sites are indicated in figure 6.1, which shows a bathymetry[33] map of the Mediterranean Sea. The site off the coast of Toulon, France is referred to as KM3NeT-Fr, and is close to where the ANTARES detector is located. The KM3NeT-It site is located off the coast of Portopalo di Capo Passero, Sicily, Italy. The third site, KM3NeT-Gr, is located off the coast of Pylos, Peloponnese, Greece.

[33] *Bathymetry is the study of underwater depth of lake or ocean floors. The name comes from the Greek words βαθός (meaning deep) and μέτρον (meaning measure).*

The detection principle of KM3NeT is the same as that of ANTARES. One key difference is that the Optical Modules (OMs) in KM3NeT will contain 31 small PMTs of 3″ diameter instead of one large PMT, see also figure 6.2. The main advantages are a 4π coverage, a very large photocathode surface and insensitivity to the Earth's magnetic field [Margiotta, 2013]. Segmenting the photocathode also helps in rejecting the background.

A prototype of the KM3NeT optical module has been attached to the instrumentation line of ANTARES, and was deployed on April 16th 2013. Data taking commenced the same day, the results of which can be found in the paper by Adrián-Martínez et al. [2014b].

Figure 6.2: Photo of the recently completed KM3NeT string. The Multi-PMT optical modules can also be seen.

Just like in ANTARES, the OMs will be attached to vertical lines that are anchored on the sea floor and held upright by buoys. A line contains 18 storeys, each containing one OM. The vertical distance between two storeys is 36 m and the first storey is located about 100 m above the sea floor. The first string has recently been completed, see the picture in figure 6.2. To facilitate the distribution over different sites, the total detector will be built up of so-called building blocks. One building block consists of 115 strings with about 90 m spacing. This number of strings and the spacing between OMs has been found to give the best detection efficiency for candidate Galactic neutrino sources while keeping the total number of optical modules constant.

The KM3NeT detector will be built in several phases. For phase 1, strings will be deployed in the Italian and French sites, and the resulting instrumented volume will be about 3 times that of ANTARES. Phase 1.5 will consist of 2 building blocks and is planned to perform an independent measurement of the neutrino

flux discovered by IceCube. The full phase 2 KM3NeT detector will consist of 6 building blocks.

More information about the technology can be found in the technical design report [Ageron et al., 2010].

6.1.1 *Muon track reconstruction*

Since the KM3NeT detector consists of different optical modules from ANTARES, new reconstruction strategies have been developed. In the following sections, the so-called RECOLNS strategy is used [Trovato, 2013]. This reconstruction strategy is based on AAFIT, which has been modified to utilise the OM properties. For example, a different hit selection is used and the charge information is substituted by the multiplicity of hits.

The first step of the reconstruction strategy is a hit selection. Each hit is assigned a score, which depends on how many other hits are in coincidence with it, and how these hits are distributed. For instance, an L1 hit (which is defined as two hits on different PMTs on the same OM within 10 ns) gets a score of 2^0, while an L3 hit (defined as a coincidence between 4 or more PMTs on the same OM within 10 ns) gets a score of 2^5. In total 6 different hit patterns are defined. The hit with the highest score, which is in 99.6% of the cases a hit caused by a passing muon, is taken as the reference hit.

After this hit selection, a causality filter is applied to remove background hits. The same causality relation as used by the 3N trigger is used for this, i. e. equation 4.10, where the allowed time difference is increased by 20 ns. Additionally, hits are required to fulfil:

$$\left| |t_i - t_j| - \frac{r_{ij}}{c} \right| < 500\,\text{ns}, \tag{6.1}$$

where r_{ij} is the distance between PMT i and j. This relation takes into account that light absorption does not allow the Čerenkov light to move far from the muon track.

The hits are then used for a linear prefit similar to that performed in AAFIT. After a first track estimate has been obtained, the angle of incidence of the photon on the PMT is determined for each hit. If this angle is larger than 60° (with 0° being a head-on hit), the hit is discarded. This improves the purity of the hit selection to about 90% [Trovato, 2013].

The result of the prefit is used as an input for an M-estimator fit, for which the function given in equation 4.34 is used. For this fit, all hits that have a time residual with respect to the prefit

between −150 ns and +150 ns and are located at most 100 m away from this track are selected. In addition, all L3 hits are selected[34].

[34] This corresponds to how hits with an amplitude larger than 2.3 p.e. are selected at ANTARES.

The third step is a Maximum Likelihood fit using the same PDF as used for AAFIT. As input all hits are selected that are at most 300 m from the M-estimator track and that have a time residual within $-0.5\,T_{\mathrm{RMS}}$ and $+T_{\mathrm{RMS}}$, where T_{RMS} is the root mean square of the residuals used for the M-estimator fit. All L3 hits are also selected again.

Step two and three are done 7200 times, by rotating the prefit track in steps of 3° and using the new track as starting point. Out of these tracks the best track is chosen according to:

$$Q = N_{\mathrm{hit}} + w\frac{\log L^{\max}}{N_{\mathrm{hit}} - 5}, \tag{6.2}$$

where N_{hit} is the number of hits used to perform the likelihood fit and $\frac{\log L^{\max}}{N_{\mathrm{hit}}-5}$ is the reduced log-likelihood (rLogL). The optimal value for the weighting factor is found to be 1.

Finally, the track with the highest value of Q is used for another Maximum Likelihood fit using the AAFIT PDF which takes the background hits into account (equation 4.42). As input, all hits with time residuals with respect to the chosen track between −150 ns and +150 ns and that are at most 100 m away from this track are selected. Again, the L3 hits are added.

Analogously to AAFIT, the angular error estimate β is defined (see equation 4.47). This parameter can be used together with the reduced log-likelihood value of the final track, to reject badly reconstructed events and misreconstructed atmospheric muons.

Although the reconstruction strategy does not perform an estimate of the muon energy, the N_{hit} parameter can be used as a rudimentary energy estimator. For instance, selecting events with $N_{\mathrm{hit}} > 30$ will select mainly events above 1 TeV; only 3% of the events below 1 TeV pass this cut [Trovato, 2013].

KM3NeT effective area

To determine the effective area for KM3NeT, the same simulation tools as described in section 4.1 are used. Background from potassium decays and the dark noise produced by the PMTs are simulated using an uncorrelated background rate of 5 kHz per PMT and a time-correlated (L1) rate of 500 Hz per optical

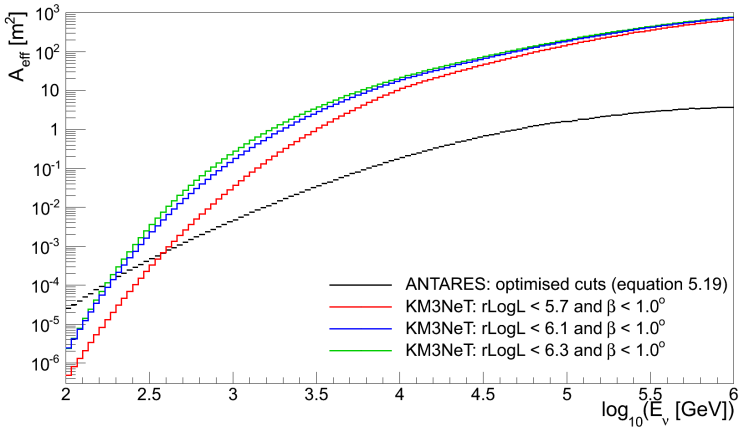

Figure 6.3: Effective area of KM3NeT phase 2 using the RECOLNS strategy for different cut combinations. Also shown is the ANTARES effective area corresponding to the event selection from equation 5.19. The average is taken for neutrinos and anti-neutrinos.

module[35].

The effective area has been determined using equation 4.25 and is shown versus neutrino energy for different cut combinations in figure 6.3. The effective area shown here is for the full phase 2 detector and the average is taken for neutrinos and anti-neutrinos. As reference, the ANTARES effective area corresponding to the event selection from equation 5.19 is shown.

[35] *This has to be added, since a KM3NeT OM consists of multiple PMTs which are situated close together, so that it is possible that the decay of ^{40}K produces a coincidence between two PMTs.*

6.2 DETERMINING THE OPTIMAL SIGNAL REGION SIZE

The detection potential of the KM3NeT detector for the diffuse Galactic neutrino flux is now assessed using the same type of analysis as used for ANTARES. Signal and background regions are defined and the corresponding numbers of events are compared. Besides optimising to obtain the best sensitivity, as is done for ANTARES, the optimisation is also done to obtain the highest probability for a discovery. This is explained in more detail below first, after which the optimisation of the size of the signal region is described in section 6.2.2.

6.2.1 *Statistical tools*

For ANTARES the optimisation of the size of the signal region has been carried out using the MRF technique, which results

in the best limit. The MRF is used, because ANTARES is too small to claim a discovery of a diffuse Galactic neutrino flux. For KM3NeT, the MDP technique is also used, which optimises the cuts for the highest probability for a discovery [Hill et al., 2005].

MDP: Model Discovery Potential

Using frequentist statistics, a discovery can be claimed if the observation is very unlikely to be caused by a background fluctuation. It is generally accepted that when this probability is smaller than $5.73 \cdot 10^{-7}$ (which is the area in the 5σ tails in a two-sided Gaussian distribution) a discovery can be claimed. When the probability is smaller than $2.7 \cdot 10^{-3}$ (the area in the 3σ tails in a two-sided Gaussian distribution) the experiment can report evidence for a new signal.

The critical number of events n^{α}_{crit} can then be defined, so that

$$P(n_{\text{obs}} \geqslant n^{\alpha}_{\text{crit}} | \, \mu_{\text{b}}) < \alpha, \tag{6.3}$$

where α is called the significance level (not to be confused with the confidence level from the MRF case), which is $5.73 \cdot 10^{-7}$ for a discovery. The critical number of events is the minimum number of events needed for an observation with a significance level of α.

If a real signal is also present, the probability to measure at least n_{crit} events is given by:

$$P(n_{\text{obs}} \geqslant n^{\alpha}_{\text{crit}} | \, \mu_{\text{b}} + \mu_{\text{s}}) = 1 - \beta, \tag{6.4}$$

where $1 - \beta$ is called the discovery potential. If for instance $1 - \beta = 0.9$, an observation of at least n_{crit} events is expected in 90% of the experiments. The least detectable signal μ_{lds} is defined to be the lowest value of μ_{s} for which the equality in equation 6.4 is satisfied. The MDP is then defined as:

$$\text{MDP} = \frac{\mu_{\text{lds}}}{\mu_{\text{s}}}, \tag{6.5}$$

and shows what level of flux the experiment can discover. By optimising the cuts to get the best MDP, the probability to make an observation at significance level α in a fraction of $1 - \beta$ experiments, is maximised.

Figure 6.4 shows the least detectable signal[36] for a 5σ observation with 50% probability as a function of the expected number of background events for different values of τ (the ratio of off-source to on-source region, see equation 5.2) and for the case with no uncertainty on the background. The same conclusion as drawn from the right plot of figure 5.1 is also valid here; the higher the value of τ (and the lower the uncertainty on the background), the lower the value of the least detectable signal.

[36] *The least detectable signal is again calculated with the profile likelihood method implemented in the* TROLKE *class in* ROOT.

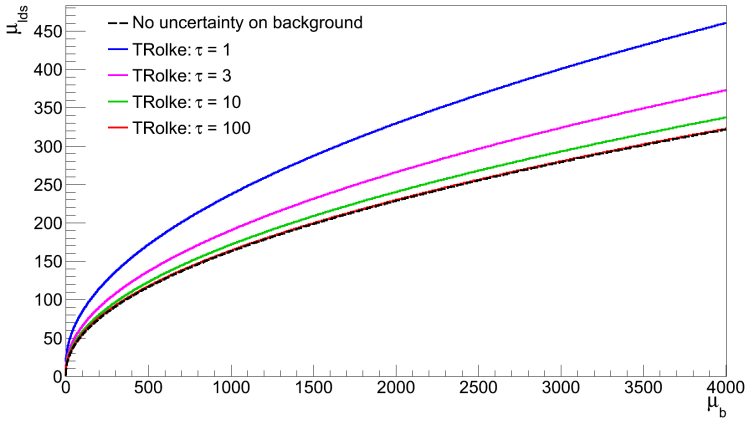

Figure 6.4: Least detectable signal for a 5σ observation with 50% probability versus number of background events for several different values of τ.

6.2.2 *Signal region optimisation*

The optimisation of the size of the signal region is again performed for different cut combinations. As before, the MRF is always calculated at 90% confidence level, whereas the MDP is calculated for a 5σ observation with 50% probability. Both the MRF and the MDP are calculated for 2 years of livetime of phase 2.

rLogL-CUT	β-CUT	N_{hit}-CUT	PURITY
5.7	1.0°	—	$> 99\%$
5.7	2.0°	—	$> 99\%$
6.1	1.0°	—	~97%
6.2	1.0°	—	~88%
6.2	2.0°	—	~88%
6.2	—	27	~86%
6.3	1.0°	—	~64%

Table 6.1: The different cut combinations considered for the signal region optimisation.

As input, the expected number of signal and background events is required, which are obtained from the effective area using equation 4.24. The flux $\Phi_\nu(E_\nu, \theta, \phi)$ is calculated by transforming the fluxes from Galactic coordinates to local coordinates and averaging over a full sidereal day.

For the optimisation, the longitude bound is again varied from 24° to 75° in steps of 3° and the latitude bound from 1° to 7.5° in steps of 0.5° and the MRF and MDP values are calculated for each combination. Several cut combinations are used for the optimisation, which are shown in table 6.1. As before, only events that are reconstructed as upgoing are considered.

MRF optimisation

Figure 6.5 shows the MRF as a function of longitude bound and latitude bound for an event selection with rLogL < 6.1 and $\beta < 1.0°$ for all four of the signal flux models. The colour scale shows the value of the MRF, with the blue part of the scale corresponding to the bottom 10% of the MRF values.

With this particular cut combination, the lowest MRF is found at $l_{\text{bound}} = 66°$ and $b_{\text{bound}} = 2.5°$ for both NoDrift models, at $l_{\text{bound}} = 42°$ and $b_{\text{bound}} = 4°$ for the Drift model and at $l_{\text{bound}} = 39°$ and $b_{\text{bound}} = 1.5°$ for the Fermi $\gamma \to \nu$ model. As before, the minimum is quite shallow, so varying the longitude or latitude bound will result in only a slightly worse MRF value.

As found in the optimisation for ANTARES, the optimal region is different for the NoDrift and the other two models, which is due to the angular distribution of the flux. Choosing the region that is optimal for the Drift model gives a 12% worse result for the NoDrift models and a 17% worse result for the Fermi $\gamma \to \nu$ model.

The influence of the cuts on the optimal region size is small, as can be seen from table 6.2, in which the MRF results for the Drift model are summarised. The influence of the atmospheric neutrino flux uncertainty is also small, resulting in the same optimal region for nearly all cut combinations. In the table, only the results for the default atmospheric neutrino flux are shown.

Concerning the event selection, the lowest MRF is obtained for rLogL < 6.1 and $\beta < 1.0°$, so this cut combination is used to assess the sensitivity of KM3NeT to the diffuse Galactic neutrino flux. It is possible to optimise the cuts further, as is done for

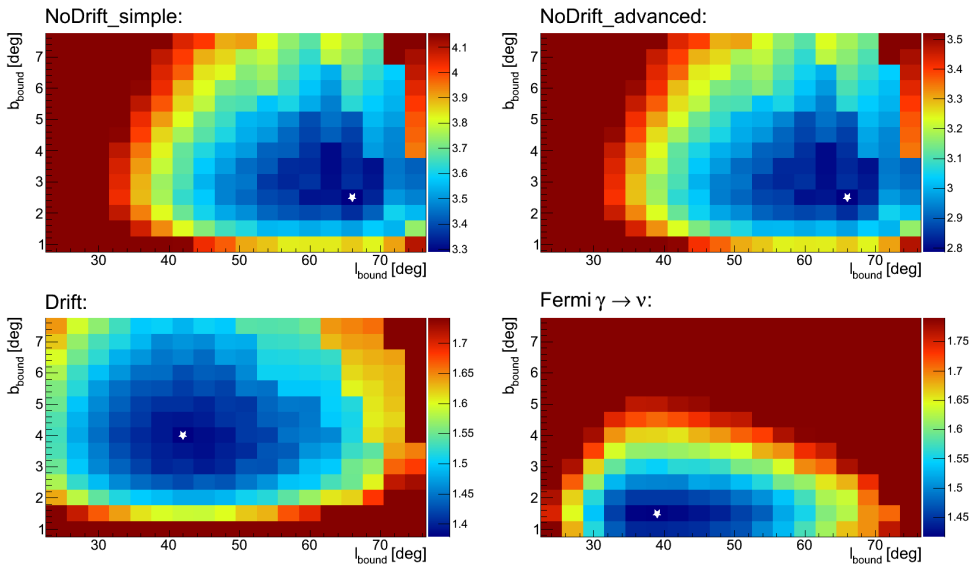

Figure 6.5: MRF versus longitude and latitude bound for an event selection with rLogL < 6.1 and $\beta < 1.0^\circ$. The white star marks the location of the minimum.

CUT COMBINATION	OPTIMAL VALUES l_{bound}	b_{bound}	MRF	μ_s	μ_b
rLogL < 5.7, $\beta < 1.0^\circ$	45°	3.5°	1.57	29.2	576
rLogL < 5.7, $\beta < 2.0^\circ$	42°	4°	1.58	30.3	624
rLogL < 6.1, $\beta < 1.0^\circ$	42°	4°	1.38	59.3	1860
rLogL < 6.2, $\beta < 1.0^\circ$	42°	4°	1.41	66.1	2420
rLogL < 6.2, $\beta < 2.0^\circ$	42°	4°	1.39	67.4	2460
rLogL < 6.2, $N_{\text{hit}} > 27$	42°	4°	1.40	66.3	2380
rLogL < 6.3, $\beta < 1.0^\circ$	45°	3.5°	1.61	71.1	3670

Table 6.2: Optimal longitude and latitude bounds and obtained MRF values for the considered cuts for the Drift model.

ANTARES, but this is beyond the scope of this work. It should be noted that it is possible to improve the senstivities shown in section 6.3.

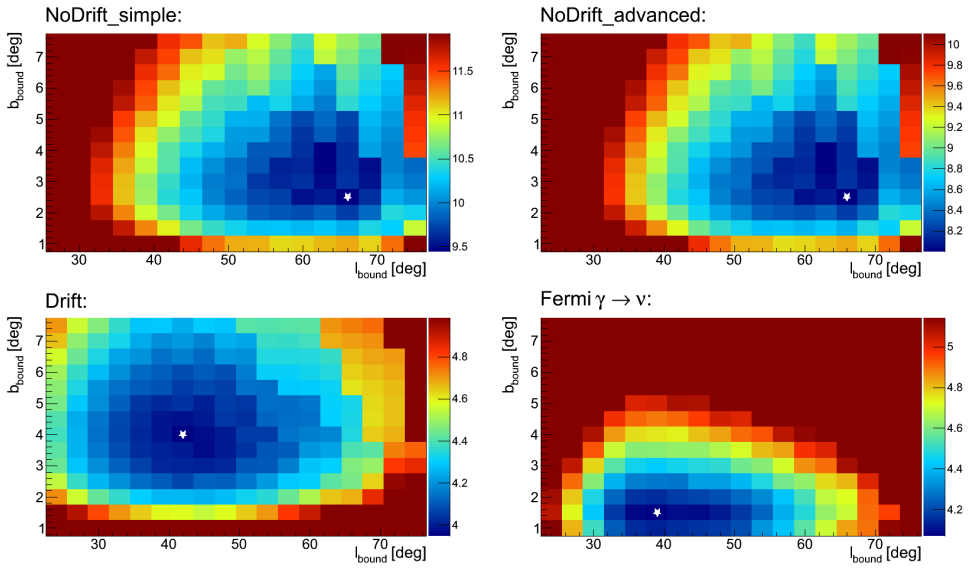

Figure 6.6: MDP versus longitude and latitude bound for rLogL < 6.1 and $\beta < 1.0^\circ$. The white star marks the location of the minimum.

MDP optimisation

The results for the MDP optimisation are shown in figure 6.6 for an event selection with rLogL < 6.1 and $\beta < 1.0^\circ$. This figure shows the MDP, calculated according to equation 6.5, versus longitude and latitude bound. The colour scale again shows the value of the MDP, with the blue part of the scale corresponding to the bottom 10% of the values. With the applied cuts, the lowest MDP is found at $l_{\text{bound}} = 66^\circ$ and $b_{\text{bound}} = 2.5^\circ$ for both NoDrift models, at $l_{\text{bound}} = 42^\circ$ and $b_{\text{bound}} = 4^\circ$ for the Drift model and at $l_{\text{bound}} = 39^\circ$ and $b_{\text{bound}} = 1.5^\circ$ for the Fermi $\gamma \to \nu$ model.

Upon comparison with figure 6.5, it can be seen that the plots are basically identical, except that the MDP values are higher than the MRF values. This means that a higher flux is needed to claim a discovery than to set a limit (for the chosen confidence level and discovery potential).

The MDP results for three of the cut combinations are shown in table 6.3 for each of the four signal models. As with the MRF case, the influence of the cuts on the optimal size of the signal region is small. The effect of the atmospheric neutrino flux uncertainty is also small, resulting in almost the same optimal size for the signal region as that found for the default atmospheric neutrino flux.

MODEL NAME	CUT COMBINATION	OPTIMAL VALUES l_{bound}	b_{bound}	MDP	μ_s	μ_b
NoDrift_simple	rLogL < 6.1, $\beta < 1.0°$	66°	2.5°	9.44	25.8	1800
	rLogL < 6.2, $\beta < 1.0°$	66°	2.5°	9.60	28.8	2340
	rLogL < 6.2, $N_{\text{hit}} > 27$	66°	2.5°	9.51	28.9	2300
NoDrift_advanced	rLogL < 6.1, $\beta < 1.0°$	66°	2.5°	8.00	30.5	1800
	rLogL < 6.2, $\beta < 1.0°$	66°	2.5°	8.08	34.3	2340
	rLogL < 6.2, $N_{\text{hit}} > 27$	66°	2.5°	8.02	34.2	2300
Drift	rLogL < 6.1, $\beta < 1.0°$	42°	4°	3.95	59.3	1860
	rLogL < 6.2, $\beta < 1.0°$	42°	4°	4.03	66.1	2420
	rLogL < 6.2, $N_{\text{hit}} > 27$	42°	4°	3.99	66.3	2380
Fermi $\gamma \to \nu$	rLogL < 6.1, $\beta < 1.0°$	39°	1.5°	4.07	33.3	648
	rLogL < 6.2, $\beta < 1.0°$	36°	1.5°	4.15	35.6	778
	rLogL < 6.2, $N_{\text{hit}} > 27$	36°	1.5°	4.11	35.7	765

Table 6.3: Optimal longitude and latitude bounds and obtained MDP value for the considered cuts for each of the signal models.

Also in this case, choosing the region that is optimal for one model, gives worse results for the others. For instance, choosing the optimal region for the Drift model, yields a 12% worse MDP for the NoDrift models and a 17% worse result for the Fermi $\gamma \to \nu$ model (which are similar percentages as found in the MRF optimisation). Since the goal is to assess the discovery potential of KM3NeT, the region that is optimal for a given model is used as signal region to assess the discovery potential of that model. For the Drift model $l_{\text{bound}} = 42°$ and $b_{\text{bound}} = 4°$ is used, for which 8 background regions can be defined and for the Fermi $\gamma \to \nu$ model $l_{\text{bound}} = 39°$ and $b_{\text{bound}} = 1.5°$ is used, for which 17 background regions can be defined. The NoDrift models are not used in assessing the discovery potential of KM3NeT, since many simplifying assumptions are made in these two models.

Again, the best results are obtained for rLogL < 6.1 and $\beta < 1.0°$, so this cut combination is also used for the discovery potential calculations. Again it should be kept in mind that the cuts can be further optimised. Furthermore, the use of an energy estimator will improve the probability of a discovery over the simple cut-and-count analysis used here. The excess of events from the diffuse Galactic neutrino flux is expected at high ener-

gies (see also figure 2.27), so taking only events above a minimum reconstructed energy value into account will improve the signal-to-background ratio. This is beyond the scope of this work and is not investigated further.

6.3 KM3NET SENSITIVITY

The sensitivity of KM3NeT to the diffuse Galactic neutrino flux has been evaluated in a model independent way using the same method as used for ANTARES. Starting from equation 5.21, the average flux upper limit is calculated for spectral indices of 2.5, 2.6 and 2.7. The energy ranges which contain the central 90% of the signal are shown in table 6.4. Comparing these results to those for ANTARES (table 5.13), it can be seen that the energy ranges are shifted towards higher energies for KM3NeT. This is due to the difference between the effective areas, which for KM3NeT rises more, but at higher energies, as can be seen from figure 6.3.

SPECTRAL INDEX	ENERGY VALIDITY RANGE
2.5	1.1 TeV − 180 TeV
2.6	0.96 TeV − 130 TeV
2.7	0.89 TeV − 96 TeV

Table 6.4: The energy validity range for the sensitivity of KM3NeT for different values of γ.

The KM3NeT sensitivities for $\gamma = 2.6$ for 1 and 10 years of livetime are shown in figure 6.7 versus neutrino energy, together with the limit and sensitivity of ANTARES. From the figure it can be seen that even with 1 year of data of the full KM3NeT detector, the obtained sensitivity is more than a factor of 7 better than that of ANTARES. Between 3 to 4 years of data taking with the full KM3NeT detector is required to reach sensitivities comparable to the fluxes predicted by the Drift model.

The same conclusion can be drawn from figure 6.8, which shows the KM3NeT sensitivity for $\gamma = 2.7$ versus Galactic longitude. In this case, 1 year of data from KM3NeT gives a sensitivity that is about 6.6 times better than the ANTARES sensitivity and a factor of about 4.4 better than the AMANDA-II limit. The reason that the improvement of the KM3NeT sensitivity to the ANTARES sensitivity is slightly smaller in this case is due to the assumed softer energy spectrum.

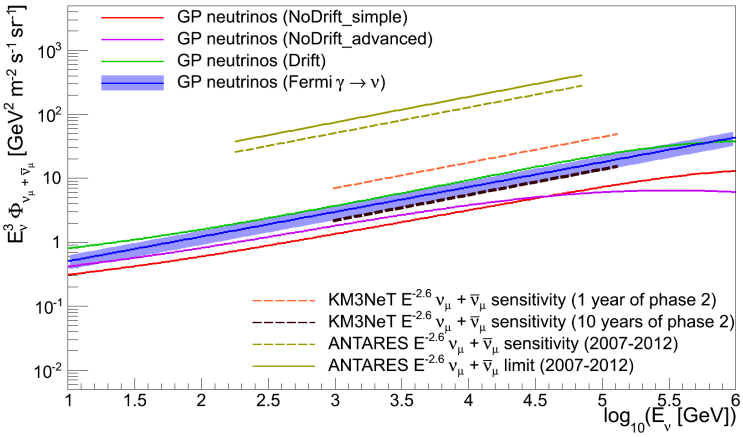

Figure 6.7: KM3NeT sensitivity versus neutrino energy for $\gamma = 2.6$ together with the average fluxes from the four signal models and the ANTARES limit and sensitivity.

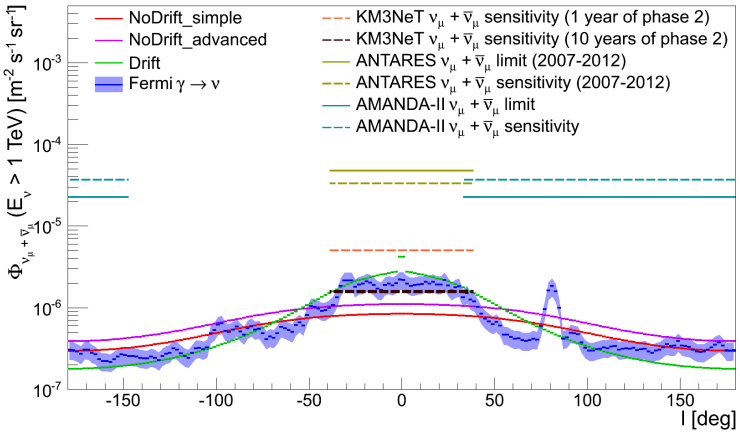

Figure 6.8: Sensitivities and limits versus Galactic longitude together with the average signal fluxes ($|b| < 4.5°$) above 1 TeV.

The evolution of the sensitivity with the number of years of data is shown in figure 6.9. The grey band represents the uncertainty on the atmospheric neutrino flux (i. e. $\pm 25\%$). The left plot shows the average upper limit that can be set on the flux constant for a spectrum with a spectral index of $\gamma = 2.6$. The right plot in the figure shows the upper limit for a spectral index of $\gamma = 2.7$. The results from the ANTARES experiment (from tables 5.13 and 5.14) and the AMANDA-II limit (equation 5.22) are also shown.

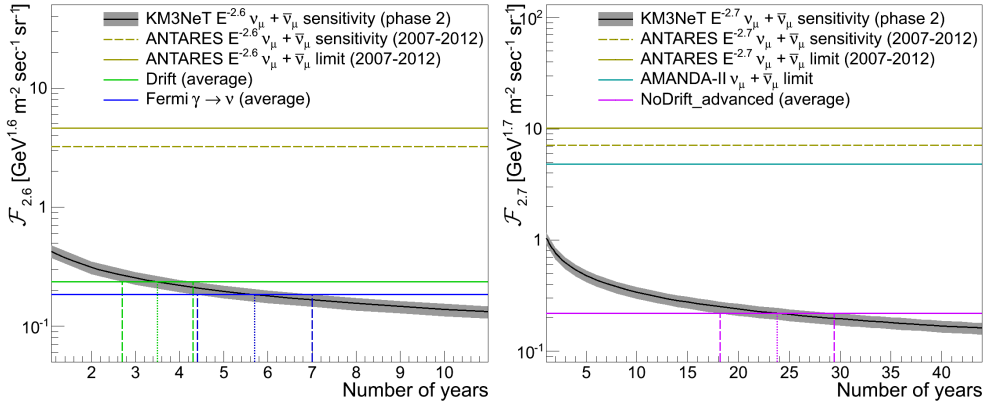

Figure 6.9: KM3NeT sensitivity versus number of years of livetime. The vertical lines denote the number of years required for the sensitivity to reach the model prediction with the same colour. LEFT: for $\gamma = 2.6$. RIGHT: for $\gamma = 2.7$.

In order to compare the KM3NeT sensitivity to the predictions from the theoretical models, a fit has been performed to the average fluxes in the signal region ($l_{\text{bound}} = 39^\circ$ and $b_{\text{bound}} = 4.5^\circ$) in order to determine the predicted flux constants. The resulting flux constants for the Drift and Fermi $\gamma \to \nu$ models are shown in the left plot and the flux constant for the NoDrift_advanced model is shown in the right plot. The spectral index predicted by the models is not exactly 2.6 (or 2.7), see table 2.3, so the fit has been performed by fixing the spectral index[37] to the value used in the plot.

The vertical lines in the figure show the number of years it takes for the sensitivity to reach the level of the flux predicted by the model. Depending on the normalisation of the atmospheric neutrino flux, this is about 2.7 to 4.3 years for the Drift model and about 4.4 to 7.0 years for the Fermi $\gamma \to \nu$ model. For the NoDrift_advanced model it would take more than 20 years to reach the level of the predicted flux. However, as remarked before, this model is not realistic.

Even though the number of years needed for KM3NeT to reach the flux predictions of the Drift and Fermi $\gamma \to \nu$ models is significant, the calculations here show that it is possible to constrain the diffuse Galactic neutrino flux. It should be noted that the sensitivity is calculated using only track-like events (i. e. from CC muon-neutrino interactions) and no real cut optimisation has been performed. Further improvements are thus possible, which are discussed in the next section.

[37] *The result for the NoDrift_simple model is not shown in either of the plots since the spectral index of 2.63 is in between the two chosen spectral indices.*

6.4 KM3NET DISCOVERY POTENTIAL

The results of the discovery potential calculation for KM3NeT are shown in figure 6.10. In the plot the significance (in number of σ) is shown versus number of years of data taken with KM3NeT. As in the MDP optimisation, the results are shown for an observation with 50% probability.

Considering the results for the most optimistic model (the Drift model), it can be seen that it takes about 30 years to reach a significance of 5σ for the claim of a discovery for this particular model. The evidence for a new signal, i. e. a significance of 3σ, takes about 11 years. The results for the Fermi $\gamma \rightarrow \nu$ model are very similar; it takes about 11 (32) years to have a significance of 3σ (5σ).

From these results it is clear that observing the diffuse Galactic neutrino flux is difficult, even for KM3NeT. However, as remarked at the end of the previous section, no real optimisation has been performed for the results presented here. In addition, only track-like events, originating from CC muon-(anti-)neutrino interactions, are considered. The sensitivity[38] can be improved in multiple ways, including:

A. Inclusion of shower-like events;

B. Flavour identification (ν_τ);

C. Using an energy estimator;

D. Optimisation of the quality cuts.

[38] *It may seem confusing that the word 'sensitivity' is used here while the discovery potential is assessed, but a 2 times lower sensitivity just means that twice as many signal events are observed for the same number of background events.*

The biggest improvement of the sensitivity is expected from the inclusion of the shower-like events. To get an estimate of the expected improvement, the results from the diffuse flux analyses in ANTARES can be used. The sensitivity of the track analysis (using only CC muon-(anti-)neutrino interactions) for 885 days of livetime is [Schnabel, 2013a]:

$$\Phi_{\nu_\mu+\overline{\nu}_\mu} < 4.70 \cdot 10^{-4}\, E_\nu^{-2}\, \mathrm{GeV}^{-1}\, \mathrm{m}^{-2}\, \mathrm{sr}^{-1}\, \mathrm{s}^{-1}, \tag{6.6}$$

with E_ν in GeV, while the sensitivity of the shower analysis for 1247 days of livetime is [Folger, 2014]:

$$\Phi_{\nu+\overline{\nu}} < 2.21 \cdot 10^{-4}\, E_\nu^{-2}\, \mathrm{GeV}^{-1}\, \mathrm{m}^{-2}\, \mathrm{sr}^{-1}\, \mathrm{s}^{-1}, \tag{6.7}$$

which is per neutrino flavour and has been calculated using the Feldman-Cousins method. Part of the improvement in sensitivity is due to the larger livetime of the data sample that is used.

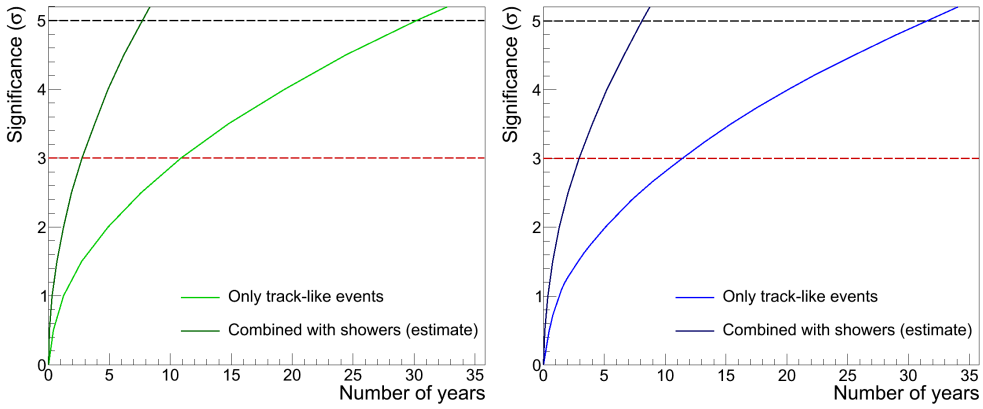

Figure 6.10: Significance obtained in 50% of the experiments versus number of years of livetime of KM3NeT. LEFT: for the Drift model. RIGHT: for the Fermi $\gamma \rightarrow \nu$ model.

Scaling the sensitivity of the showers to 885 days of livetime gives:

$$\Phi_{\nu+\overline{\nu}} < 2.81 \cdot 10^{-4} \, E_{\nu}^{-2} \, \mathrm{GeV}^{-1} \, \mathrm{m}^{-2} \, \mathrm{sr}^{-1} \, \mathrm{s}^{-1}, \tag{6.8}$$

which is an improvement of about 70% compared to the analysis using track-like events. It should be noted that this improvement is obtained by using shower-like events *instead* of track-like events. A combination of both will improve the sensitivity even further. From these considerations, a sensitivity improvement of a factor of 2 compared to that obtained here seems realistic.

The curves for the significance versus number of years when including shower-like events (i. e. a sensitivity improvement of a factor 2) are also shown in the plots in figure 6.10. It can be seen that a significance of 3σ is reached for the Drift model after only 2.8 years of data taking and a significance of 5σ after about 7.7. Again, the results for the Fermi $\gamma \rightarrow \nu$ model are similar; it takes 2.9 (8.1) years of taking data to reach a significance of 3σ (5σ).

Optimisation of the quality cuts, flavour identification of the neutrinos and usage of an energy estimator could result in further improvements, reducing the amount of time needed for a discovery.

A complication in assessing the discovery potential is the neutrino flux measured by IceCube. Since the origin of this flux is not known at the time of writing, it is not known how it will affect the analysis of the diffuse Galactic neutrino flux. As described in section 5.4.1, if the flux is truly diffuse, the same number of events are expected in the signal region and each of the background

regions. In this case, the flux measured by IceCube constitutes an additional background. If, however, the flux is Galactic in origin (or at least has a strong Galactic component), the number of events in the signal region will be higher and this will enhance the obtained significance. The two flux contributions then have to be disentangled, which requires a better modelling of the diffuse Galactic neutrino flux.

In summary, it is difficult to predict how many years of data of KM3NeT are required for a discovery. It is clear, however, that the measurement of the diffuse Galactic neutrino flux requires a combined track and shower analysis. The presented results show that with KM3NeT it should be possible to study the diffuse Galactic neutrino flux after about 3 years of operation.